Research on Chemical Intermediates (2024) 50:1081–1111
https://doi.org/10.1007/s11164-023-05124-1

Synthesis, spectral characterisation, in vitro cytotoxicity, antimicrobial, antioxidant, DFT and molecular docking studies of Ru(III) complexes derived from amide-based macrocyclic ligands

Subhash · Jyoti[2] · Monika Gupta[3] · Anita Phor[4] · Ashu Chaudhary[1]

Received: 17 July 2023 / Accepted: 26 August 2023 / Published online: 19 September 2023

Abstract

It is absolutely essential to combat some classes of tumours since they are thought to pose major health risks, necessitating the discovery and development of efficient anticancer medicines. Ruthenium coordination compounds have demonstrated a promising anticancer and antibacterial activity. Novel tetradentate macrocyclic ligands ($TAMacL_1$–$TAMacL_3$) and their Ru(III) complexes were synthesised by condensation of 4-bromobenzene-1,2-diamine with dicarboxylic acid. Analytical techniques and diverse spectroscopy equipment, including infrared, magnetic, thermal, ^{1}H NMR, ^{13}C NMR, electronic, PXRD, and mass spectra, were used to characterise the compounds. It was discovered that the complexes' geometrical structure was distorted octahedral. Density functional theory (DFT) at the B3LYP level was used to optimise the molecular geometries of the ligands and the metal complexes. The LUMOs' energy was connected to their biological activities. The antibacterial efficacy of the ligands ($TAMacL_1$–$TAMacL_3$) and their Ru(III) complexes against various bacterial Gram+ve (*S. mutans* and *S. aureus*), Gram−ve bacterial strains (*K. pneumoniae* and *E. coli*) and fungi (*F. oxysporum* and *C. albicans*) species has been investigated. The antioxidant capacity was assessed using the DPPH free radical test, with an IC_{50} range of 0.414–0.205 L and a range of 26.21–66.86%. The significant bioactivity of all synthesised compounds was observed to increase with chelation due to the process of charge transfer from metal to ligand. Our synthesised compounds' anticancer effects might be related to a mechanism that interferes with DNA replication rather than DNA cleavage, comparable to that of 5 fluorouracil. The

✉ Ashu Chaudhary
ashuchaudhary21@gmail.com

[1] Department of Chemistry, Kurukshetra University, Kurukshetra, Haryana 136119, India

[2] Department of Applied Science, UIET, Kurukshetra University, Kurukshetra, Haryana 136119, India

[3] Department of Chemistry, Vaish College, Rohtak, Haryana 124001, India

[4] Department of Chemistry, Hindu College Sonipat, Sonipat, Haryana 131001, India

interaction of the macrocyclic compounds with the target proteins' receptor active sites was also determined using molecular docking (PDB IDs 3T88, 6WII, 3TY7, 3L8R, 3DRA, and 8EBB). The molecular docking and several biological research were connected with one another. The research presented here proposes using these ligands and complexes in the creation of novel anticancer medications.

Graphical abstract

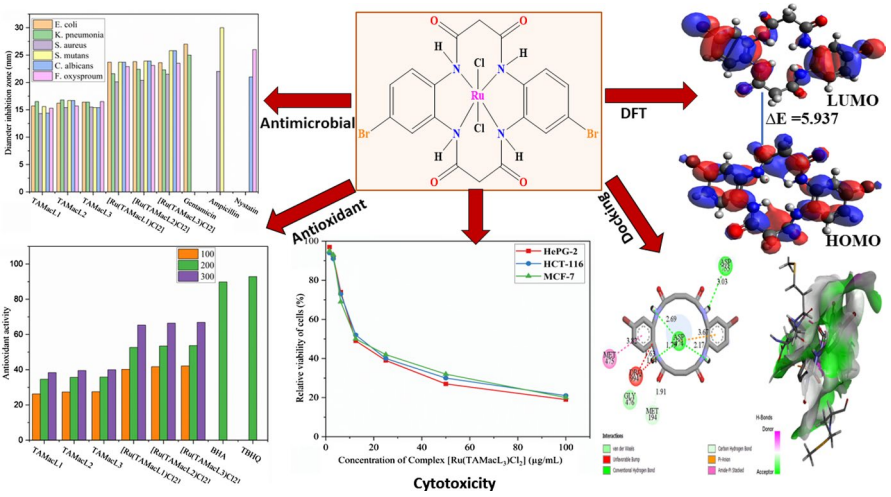

Keywords Cytotoxicity · Antimicrobial · DFT investigation · Molecular docking · Ruthenium (III) · Thermal analysis

Introduction

Metallopharmaceuticals have traditionally employed coordination chemicals. It is possible to create novel chemistries with these metals in ligand systems, as evidenced by the many roles that transition metals complexes of amide-based macrocyclic ligands play in biological systems. [1, 2]. N-donor metal complexes have drawn a lot of interest because of their fascinating chemical properties and possible biological uses. Due to their industrial, carcinostatic, anticancer, antiviral, and antimalarial activity, complexes of ligands containing N_4 donor sequences are of great interest. [3]. Among the various approaches invented for combating this issue, the discovery of novel medicines with higher activity and different ways of exposure is more beneficial for researchers [4].

It is vital to structurally optimise or modify current antibiotics to increase their range of activity and binding affinity while preserving their safety profiles and bioavailability in order to combat the fast emergence of drug resistance in microorganisms [5]. Pharmacologically significant compounds have been developed using heterocyclic ring structures. It has been established that heterocyclic

molecules with oxygen and nitrogen are physiologically active [6]. The past 10 years have seen an increase in the synthesis of heterocyclic compounds with high nitrogen contents due to their potential uses in a variety of domains, particularly medical chemistry [7]. The kind of coordinating ligands, the oxidation state of the central metal ion, and the coordination geometry of the metal complexes all affect the reactivity of transition metal chelates [8]. One of the main drivers behind the search for new effective medicines to stop bacterial development is the existence of antibiotic resistance [9]. Because both the ligands and the metal ions have the capacity to affect different phases of pathogenic life cycles, the metal ions complexed with bioactive substances are more effective [10]. Because research into the theoretical modelling of drug creation has taken front stage in recent years, computational chemistry has attracted a lot of interest. In theoretical molecular modelling, density functional theory (DFT) has taken off like a meteor. Many molecular characteristics may be calculated using the DFT approach with more accuracy than with the conventionally coupled ab initio methods, and at a more affordable computing cost [11]. A review of the literature revealed that DFT has significant accuracy in replicating the values for the geometrical structure that are indicated experimentally [12].

Transition metal ions are regarded as crucial ions in bodily biological processes [13]. For instance, people have high levels of zinc (II), nickel (II), and copper (II). They can be located in the active sites of many enzymes [14] or as structural elements of such enzymes. On the other hand, polyamines in general, including diamines and triamines, are good complexing agents and may coordinate to a variety of transition metal ions [15]. Therefore, by coordinating certain metal ions to them, the physiological relevance of organic molecules with nitrogen donors and their active function was growing [16]. As a result, transition metal complexes are crucial to many biological processes [17–19]. Metal ions have been found to have a significant impact on the antibacterial and antifungal properties of antibiotics [20]. Ruthenium (III) and (II) tetraamines (d^5 and $d.^6$) represent an interesting area of research in medicinal chemistry due to their solubility, stability in aqueous media, and biological activity [21, 22].

Consequently, in light of the foregoing details and as a continuation of our earlier work on the synthesis of macrocyclic complexes [23], Herein, we define the synthesis, characterisation and molecular modelling of tetraamide macrocyclic-ligands ($TAMacL_1$–$TAMacL_3$) and associated [Ru(III)($TAMacL_1$)Cl_2]-[Ru(III)($TAMacL_3$)Cl_2] complexes. The freshly synthesised complexes are characterised using a variety of physico-chemical and spectroscopic approaches However, calculations using the density functional theory (DFT) have been done to support the optimised geometrical shapes of compounds. Additionally, against several cancer cell lines and harmful microbe strains, the anticancer and antimicrobial properties of the ligands ($TAMacL_1$–$TAMacL_3$) and their corresponding Ru(III) complexes are assessed. Moreover, DPPH tests are used to evaluate their antioxidant capabilities. We also found that molecular docking results are in the good agreement with the experimental findings.

Experimental section

Material and methods

Methanol, 4-bromobenzene-1,2-diamine, dicarboxylic acids (malonic acid, succinic acid, glutaric acid), and ruthenium chloride were the compounds and solvents employed in this study. All chemicals were procured from Merck. Using KBr discs and a Unicam Mattson 1000 FTIR spectrometer, infrared measurements were taken (4000–200 cm^{-1}. A Perkin-Elmer UV–visible Spectrophotometer Lambda 25 in DMSO was used to record UV–visible spectra, and an elemental analysis was performed using a Vario EL III CHNS analyzer. A model-306 Systronics conductivity bridge was used to evaluate the molar conductance of metal complexes in dry DMF with a concentration of 1×10^{-3} M. The experiment was done at room temperature [24]. At room temperature, EPR spectra of powdered materials were recorded using a JEOL-FA200 ESR spectrophotometer at X-band frequencies, and DPPH was utilised as a field maker (g 2.0036). Shimadzu TGA-50H thermal analyzer with 10 Celsius/min. was used to perform thermogravimetric analysis in inert environment $N_2$with flow of 20 cm^3 min^1. The current substances' mass spectra (in m/z) were found using a waters Q-tof Micro YA263 mass spectrometer. The API 2000 mass spectrometer, which has a Shimadzu Prominence LC and an electrospray source, was used to record the mass spectra. ^{1}H-NMR and ^{13}C NMR spectra were recorded in DMSO solvent on JEOL ECZS NMR instrument.

Synthetic process

Macrocyclic Ligands ($TAMacL_1$–$TAMacL_3$)

For the synthesis of ligand $TAMacL_1$, the ethanolic solutions of 4-bromobenzene-1,2-diamine (20 mmol, 3.740 g) and adipic acid (2.081 g, 20 mmol) were reflexed in 100-ml RB (round bottom) flask in 2:2 molar ratios for 8–9 h in the presence of conc. HCl at 75–80 °C. After the contents were cooled, a light brown crystalline substance that had been present overnight at 0 °C separated. The reaction was monitored by TLC using petroleum ether, ethyl acetate, toluene, and methanol solvents and recrystallised by using the solvent ethanol and benzene. It underwent filtering, several cold MeOH washes, and vacuum drying over P_4O_{10}. For the synthesis of macrocyclic ligands $TAMmacL_2$ and $TAMacL_3$, the same method was followed using succinic (2.361 g, 20 mmol) and glutaric acid (2.642 g, 20 mmol), respectively, instead of adipic acid (Scheme 1) [25].

$TAMacL_1$ (2,12-dibromo-5,9,14,18-tetrahydrodibenzo[b,i]1,4,8,11]tetraazacyclotetradecine-tetraone)
$TAMacL_2$ (2,13-dibromo,octahydrodibenzo[b,j][1,4,9,12]tetraazacyclotetradecine-6,9,16,19-tetraone)
$TAMacL_3$ (2,14-dibromo,octahydrodibenzo[*b,k*][1,4,10,13]tetraazacyclotetradecine-6,10,17,21-tetraone)

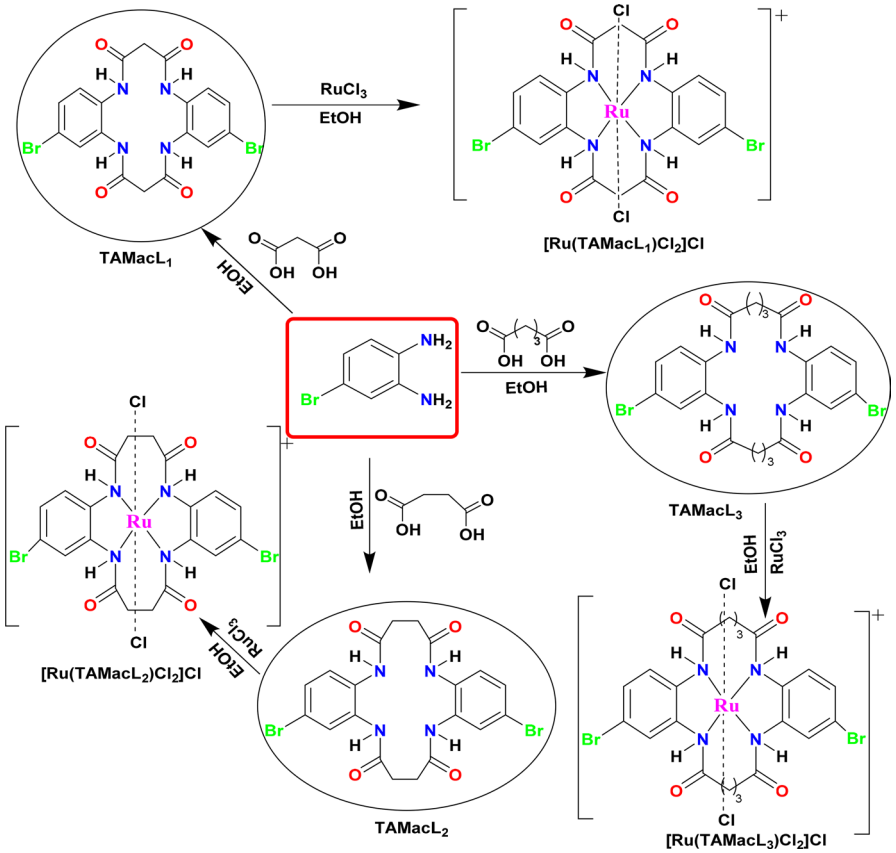

Scheme 1 Synthetic process of macrocyclic ligands and their Ru(III) complexes

Macrocyclic Complexes [Ru(III)($TAMacL_1$)Cl_2]-[Ru(III)($TAMacL_3$)Cl_2]

For the synthesis of macrocyclic complex [Ru(III)($TAMacL_1$)Cl_2]Cl, the hot ethanolic solutions of $RuCl_3$ (1 mmol, 0.2254 g) and macrocyclic ligand $TAMacL_1$ (0.5079 g, 1 mmol) were refluxed in 100-ml RB (round bottom) flask at 80 °C for 9–10 h in 1:1 metal-to-ligand ratio. A coloured complex was formed after cooling, and these were undergoing filtering, several cold MeOH washes, and vacuum drying over P_4O_{10}. TLC was used to monitor the reaction, which was carried out with petroleum ether, ethyl acetate, toluene, and methanol as solvents and recrystallised with ethanol and benzene as solvents. For the synthesis of macrocyclic complexes [Ru($TAMacL_2$)Cl_2] and [Ru($TAMacL_3$)Cl_2], the same method was followed using $TAMacL_2$ (0.66 g, 1 mmol) and $TAMacL_3$ (0.69 g, 1 mmol) macrocyclic ligands, respectively, instead of $TAMacL_1$ [26].

[Ru(III)($TAMacL_1$)Cl_2]Cl (2,12-dibromo,tetrahydrodibenzo[b,i]1,4,8,11] tetraazacyclotetradecine-tetraone,dichloro-ruthenium(III)chloride).

[Ru(III)(TAMacL$_2$)Cl$_2$]Cl (2,13-dibromo,octahydrodibenzo[b,j][1,4,9,12] tetraazacyclotetradecine-6,9,16,19-tetraone,dichloro-ruthenium(III)chloride).
[Ru(III)(TAMacL$_3$)Cl$_2$]Cl (2,14-dibromo,octahydrodibenzo[*b,k*][1,4,10,13] tetraazacyclotetradecine-6,10,17,21-tetraone,dichloro-ruthenium(III)chloride).

Quantum chemical calculations

Using the DFT method, the macrocyclic ligands (TAMacL$_1$–TAMacL$_3$) and Ru(III) complexes were optimised in three dimensions. An octahedral geometry was optimised for the Ru(III) complex. All DFT calculations were carried out using a hybrid functional B3LYP (Becke's three-parameter hybrid function utilising the correlation functional LYP), based on the basis sets def2-SVP for C, H, N, and O atoms as well as def2-SVPZZ for Ru atoms carried out by Avogadro 4.0 and Orca software. The terms HOMO and LUMO, respectively, stand for the electropositive and electronegative densities also used to calculate quantum chemical parameters [27, 28].

Antimicrobial activity

Antibacterial activity

The antibacterial study of synthetic compounds against (*S. aureus* and *S. mutans*) and (*E. coli* and *K. pneumoniae*) Gram+ve and Gram−ve strain, respectively [29], was performed using the agar well diffusion technique. The nutritional agar was uniformly distributed [22]. The Muller Hinton Agar medium was transferred to petri plates, and plates were swabbed with 100-µl of test microorganism inoculated and kept for 15 min for adsorption. Wells were then bored into the seeded agar plates and loaded with 100 µl of volume having concentration 15 mg/ml of each compound reconstituted in DMSO. For 24 h, all plates were incubated at 35 °C. By measuring the expansion of the inhibition zone against the test organisms using a zone reader (HI antibiotic zone scale), the antimicrobial activity of each drug was assessed. The outcomes of the compounds following zone development were contrasted with those of the common antibiotic ampicillin and gentamycin.

Antifungal activity

The agar plate technique was used to test the ligands (TAMacL$_1$–TAMacL$_3$) and Ru(III) complexes antifungal activity against the fungus *F. oxysporum* and *C. albicans* [30]. The concentrations 15 mg/ml of the chemicals were added directly to the medium. The inoculum needle was used to apply the fungus to the medium. The petri dishes were placed in an incubator at 25 °C for 96 h while being covered in polythene sheets with a limited amount of alcohol. By noting the diameter of the fungal colony, the growth of fungi was quantified. Fungal growth inhibition% $= (A_c - B_t) \times 100/A_c$, where A_c is the diameter of the fungus colony in the

control plate and B_t is the diameter of the fungus colony on the test plates after 96 h. Nystatin was used as standard to compare the antifungal activity results of the synthesised ($TAMacL_1$–$TAMacL_3$) and Ru(III) complexes.

Antioxidant activity

The described complexes' in vitro antioxidant properties were assessed by scavenging the stable 2,2-diphenyl-1-picrylhydrazyl (DPPH) radical [31]. The radical scavenging test is based on how the radical's absorbance changes when antioxidants deactivate it. The standard substance was ascorbic acid. The described complexes' stock solutions were dissolved in methanol/DMSO (5:1) before being diluted to various quantities. The solution [3.9 ml, 0.004% (w/v)] of DPPH in methanol was administered to each experiment at different concentrations (100, 200 and 300 µg ml^{-1}) of high-performance liquid chromatography (HPLC) methanol. The tubes were kept at room temperature for 30 min, and the absorbance at 517 nm was recorded. Both tests were performed in triplicate and were averaged. $SCA\% = [(A_{control} - A_{test})/A_{control})] \times 100$ where $A_{control}$ is the control absorbance (DPPH without sample) and A_{test} is the sample absorbance (DPPH plus scavenger) to describe the percentage of scavenging activity on DPPH.

Cytotoxicity

The MTT assay was used to evaluate the cytotoxic effects of the macrocyclic ligands ($TAMacL_1$–$TAMacL_3$) and their Ru(III) complexes to grown cancer cells. The NCCS Pune, India, provided three different human cancer cell lines: hepatocellular carcinoma (HePG2), colorectal carcinoma (HCT116) and mammary gland breast carcinoma (MCF7). These cell lines were used to screen the investigated compounds' in vitro anticancer activity in accordance by using the MTT assay. [32] Foetal bovine serum, MTT, DMSO, and 5 fluorouracil are the reagents that were employed. Fluorouracil was employed as a benchmark anticancer medication in this study. This test is based on the fact that, in living cells, mitochondrial succinate dehydrogenase converts the yellow tetrazolium bromide (MTT) into a purple formazan derivative. 10% foetal bovine serum was used to grow the cells in RPMI 1640 medium. Antibiotics of 100 units per ml penicillin and 100 g/ml streptomycin were introduced at 37 °C in an incubator with 5% CO_2. The cells were seeded at a density of 1.0×10^4 cells/well on a 96-well plate for 48 h at 37 °C and 5% CO_2 [33]. The cells were then exposed to various chemical concentrations and incubated for one day. Following a one-day drug incubation period, 20 L of MTT solution containing 5 mg/mL was added and incubated once more for 5 h. To dissolve the produced purple formazan, 100 L of dimethyl sulfoxide (DMSO) was applied to each well. The IC_{50} values were used to reflect the cytotoxicity of the drugs.

Molecular docking

Utilising the AutoDock and PyRx technologies, molecular docking experiments were developed. Predicting the potential binding modes of the most active drugs with the receptors of (PDB ID 3T88, 6WII, 3TY7, 3L8R, 3DRA, and 8EBB) is greatly aided by these investigations. Antibacterial targets included *E. coli* (3T88), *K. pneumonia* (6WII), *S. aureus* (3T47), and *S. mutans* (3L8R), whereas antifungal targets included *C. albicans* (3DRA) and *F. oxysporum* (8EBB). For molecular docking investigations, we chose receptors (3T88, 6WII, 3TY7, 3L8R, 3DRA, and 8EBB). The reason for choosing these five proteins is that the resolution of picking proteins is low, ensuring higher protein structure quality. These proteins are chemically similar to ligands ($TAMacL_1$–$TAMacL_3$) and their ruthenium complexes $[Ru(TAMacL_1)Cl_2]$–$[Ru(TAMacL_3)Cl_2]$. These proteins with the greatest enrichment value were chosen for docking because of their structure. The docking modes of synthesised substances and receptors may be calculated and displayed using the docking interactive molecular graphics programme [34]. The ligand and receptor must be entered in PDB format. The amino acid chain was preserved, but the water molecules, co-crystallised ligands, and other unsupported elements (Na, K, Hg, etc.) were eliminated. The ligand's structure was produced using the Avogadro 4.O programme as a PDB file. The protein data bank (http://www.rcsb.org/pdb) provided the crystal structures of (PDB ID 3T88, 6WII, 3TY7, 3L8R, 3DRA and 8EBB) *E. coli* (3T88), *K. pneumonia* (6WII), *S. aureus* (3T47), *S. mutans* (3L8R) were specified as antibacterial target, *C. albicans* (3DRA) and *F. oxysporum* (8EBB).

Results and discussion

Molar conductance

The synthesised complexes $[Ru(TAMacL_1)Cl_2]Cl$, $[Ru(TAMacL_2)Cl_2]Cl$, and $[Ru(TAMacL_3)Cl_2]Cl$ are defined as electrolytes as the conductivity values in dimethylformamide solution at the conc. of 10^{-3} M are 105, 103, and 108 Ω^{-1} cm^2 mol^{-1}, respectively, at 25 °C [35]. The conductivity of macrocyclic compounds was also measured in acetone at the conc. of 10^{-3} M and found 101–107 Ω^{-1} cm^2 mol^{-1}, which confirms the molar conductivity measurements. Accordingly, one chloride ion is found outside the coordination sphere, indicating that this complex 1:1 electrolyte has an ionic nature and supports the IR characterisation component.

IR spectra

In order to describe the structures of the macrocyclic ligands ($TAMacL_1$–$TAMacL_3$) and their octahedral complexes $[Ru(TAMacL_1)Cl_2$–$Ru(TAMacL_3)Cl_2]$ in detail, their IR spectra have been examined (Figures S1–S3). The IR spectra of compounds showed a single wide band at 3245–3275 cm^{-1} owing to v(NH) stretching vibration,

indicating the condensation of the carboxylic group of adipic acid with the amino group of 4-bromo-1,2-diaminobenzen [36]. Bands in the ligand's IR spectra that may be attributed to the amide [I ν(C=O), amide II ν(C–N) δ(N–H)], amide III δ(N–H) and amide IV wagging [(C=O)], vibration, respectively, are mostly seen in the areas of 1660–1710, 1505–1555, 1235–1260 and 630–660 cm^{-1} [37] (Fig. 1). The existence of the sec. ν(NH) group is shown by a sharp band at 3288–3302 cm^{-1}. These bands are moved to lower energy areas in comparison with the unbound macrocyclic ligands, demonstrating that the ligands coordinate to metal ions via the nitrogen atom of the (-NH) group [38]. Bands in the 454–478 cm^{-1} range were assigned as ν(M–N) presented more solid evidence for macrocyclic ligands association with the ruthenium metal. The bands in the 324–342 cm^{-1} range may have a ν(M–Cl) vibration associated with them [39] (Table 1).

^{1}H-NMR and ^{13}C-NMR spectral study

In DMSO-d6 solvent, the ^{1}H-NMR and ^{13}C-NMR spectra of amide-based macrocyclic ligands ($TAMacL_1$–$TAMacL_3$) were obtained (Fig. 2 and Figures S4–S7). A fairly wide signal for the amine protons, peaks for aromatic protons at δ 6.2–6.9 ppm, and the signal for the methyl proton show at 2.3 ppm in the ^{1}H-NMR spectrum of 4-bromobenzene-1,2-diamine. No peak could be ascribed for an –OH or an $–NH_2$ group in the ^{1}H NMR spectra of the macrocyclic ligands ($TAMacL_1$–$TAMacL_3$), supporting the development of the postulated macrocyclic ligands after condensation. The tetraamide macrocyclic ligands' ^{1}H-NMR spectra revealed a wide signal at δ 10.03–10.25 ppm that was potentially attributed to the –NH protons [40]. In macrocyclic compounds, signals may be seen around δ 6.87–8.05 ppm and δ 2.2–2.3 ppm, respectively, which correspond to aromatic protons and methyl protons in Table 2. The resonance signal at 166.05 ppm in the ^{13}C NMR spectra of macrocyclic ligand [$TAMacL_1$] belonged to the carbons connected to the nitrogen atoms and was suggestive of their proposed coordination in the ligands. However, the absence of a signal at 184 and 159 ppm, which would have shown the full condensation, confirmed the creation of the macrocyclic moiety. The signals in the ppm range of δ 115.12–135.22 ppm further demonstrated the presence of aromatic carbons in macrocyclic moiety. The signals for aliphatic carbons presented in the macrocyclic ligands in Fig. 3 [41] are seen in the range of δ 47.47–48.57 ppm (Table 3).

Electrospray ionisation mass spectra

The electrospray ionisation mass spectra of macrocyclic complex [Ru($TAMacL_1$)Cl_2] are represented in Fig. 4. The (M.F) of [Ru($TAMacL_1$)Cl_2] is ($C_{18}H_{14}Br_2RuCl_3N_4O_4$) (Mol. Wt. 717.56) in Fig. 4. The ESI-mass spectrum of complex [Ru($TAMacL_1$)Cl_2] displays the M/Z peak consistent to $[M]^+$ and $[M+2]^+$ ions. The $[M]^+$ peak is consistent to $[C_{18}H_{14}Br_2Cl_3N_4O_4]^+$ at m/z = 716.42.31 (due to ^{35}Cl) and the peak $[M+2]^+$ corresponding to $[C_{18}H_{14}Br_2Cl_2N_4O_4]^+$ at m/z = 718.4231 (due to ^{37}Cl). The results from the elemental analysis were confirmed by the molecular ion peak. Some fragmentations of macrocyclic complex

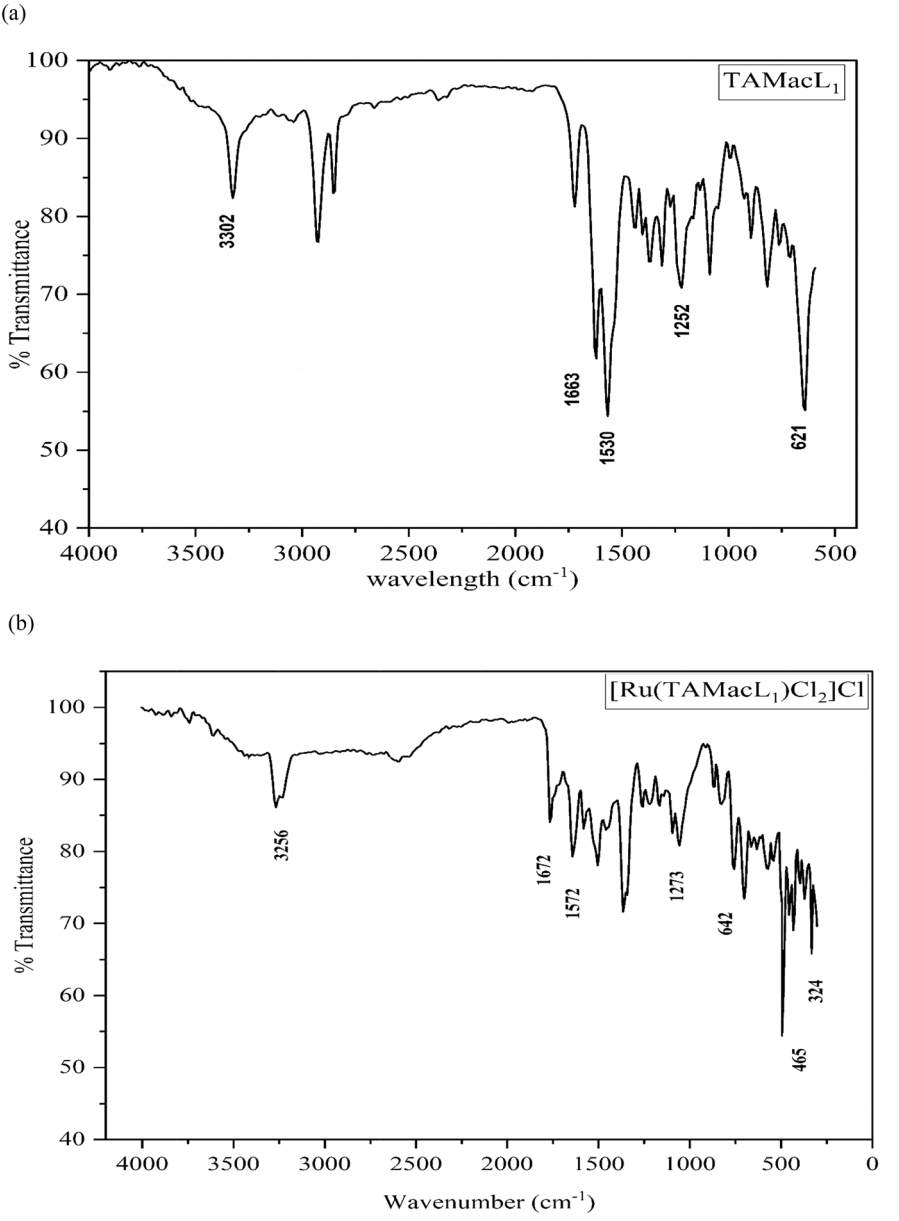

Fig. 1 IR spectra: **a** tetraamide macrocyclic ligand $TAMacL_1$, **b** complex $[Ru(TAMacL_1)Cl_2]Cl$

$[C_{18}H_{14}Br_2RuCl_2N_4O_4]$ at 682.1 $[C_{18}H_{14}Br_2N_4O_4]^+$, 612.1 $[C_{15}H_{12}Br_2RuCl_2N_4O_2]^+$, 612.05 $[C_3H_4N_2O_2]^+$, 100.08 $[C_6H_8N_4O_4]^+$, 200.05 $[C_{18}H_{14}Br_2N_4O_4]^+$, 513.3671 $[C_6H_5BrN_2]^+$, 185.02 $[C_{12}H_{10}Br_2N_4]^+$, 348.3103 $[C_4RuCl_2N_4]^+$, 276.2746 were also

Table 1 Infra-red data (cm^{-1}) of the macrocyclic ligands and Ru(III) complexes

Compound	ν(NH)	Amide				ν(Ru–N)	ν(Ru–Cl)
		I	II	III	IV		
[$TAMacL_1$]	3302	1663	1530	1252	621	–	–
[$TAMacL_2$]	3296	1671	1550	1268	631	–	–
[$TAMacL_3$]	3288	1668	1563	1270	645	–	–
[$Ru(TAMacL_1)Cl_2$]Cl	3256	1672	1572	1273	642	465	324
[$Ru(TAMacL_2)Cl_2$]Cl	3260	1684	1588	1288	651	472	332
[$Ru(TAMacL_3)Cl_2$]Cl	3255	1679	1579	1286	656	487	342

observed. The EI-MS spectra of ($TAMacL_1$–$TAMacL_3$) and their Ru(III) are represented in Figures S8-S11.

Electronic spectra

The UV–Vis spectra of ligands ($TAMacL_1$–$TAMacL_3$) reveal an absorption band in the 272–395 nm range, which may be connected to $n \rightarrow \pi^*$ transition that originates largely in the amide (>C–NH) chromophore and changes to a lower frequency during complexation. From these results, it is concluded that the nitrogen atom of amide group coordinated to the metal ion. The absorption at 388 cm^{-1} and 276 cm^{-1},

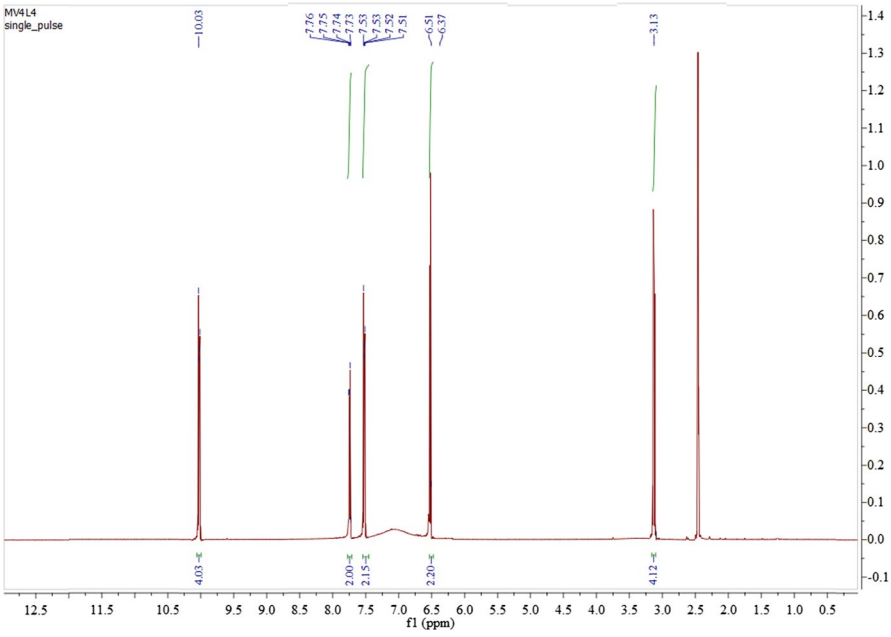

Fig. 2. ^{1}H-NMR spectrum of tetraamide macrocyclic ligand $TAMacL_1$

Table 2 ^{1}H-NMR data (in ppm) of ligands ($TAMacL_1$–$TAMacL_3$)

Compounds	(CO–NH) (m)	1,4-C_6H_4 (m)	1,2-C_6H_4 (m)	CH_2 (s)
$TAMacL_1$	10.03	7.51–7.76	6.37–6.51	3.13
$TAMacL_2$	10.25	7.42–7.53	6.33–6.49	3.36
$TAMacL_3$	10.14	7.63–7.71	6.45–6.56	3.25

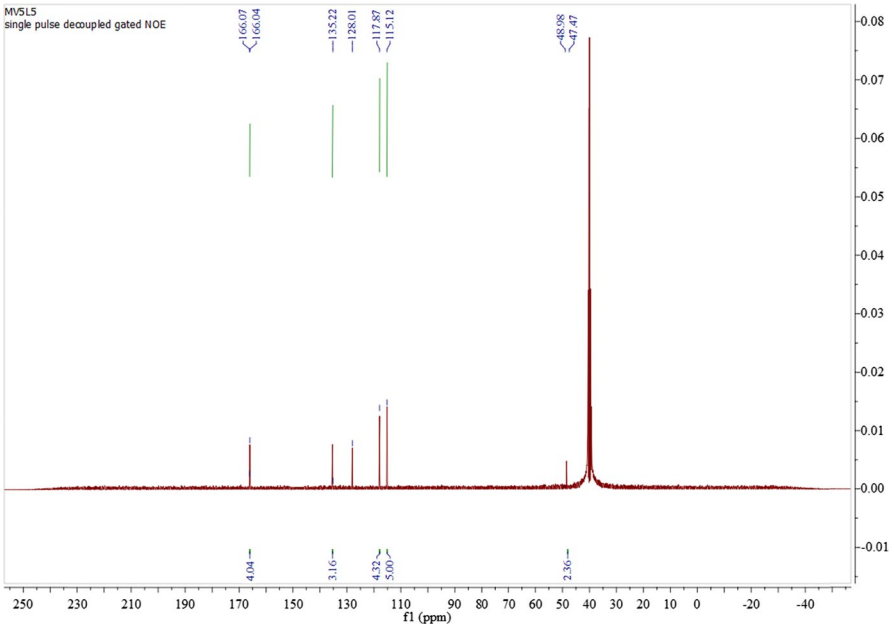

Fig. 3. ^{13}C-NMR spectrum of tetraamide macrocyclic ligand $TAMacL_1$

Table 3 ^{13}C-NMR data (in ppm) of ligands ($TAMacL_1$–$TAMacL_3$)

Compound	(CO–NH)	1,4-C_6H_4	1,2-C_6H_4	–CH_2
$TAMacL_1$	166.07	115.12, 117.87	128.01, 135.22	47.47, 48.98
$TAMacL_2$	169.08	116.18,118.45	129.74, 130.52	47.09, 48.18
$TAMacL_3$	170.51	119.92, 122.07	122.21, 122.33	48.57

which correspond to the $^{2}T_{2g} \rightarrow {}^{4}T_{1g}$ and $^{2}T_{2g} \rightarrow {}^{4}T_{2g}$ transitions, respectively, can be seen in the complex's electronic spectrum. The bands seen in the area at 531 cm^{-1} and 432 cm^{-1} are those of $\pi-\pi^*$ and $n-\pi^*$ transitions, respectively. These band locations line up with the octahedral complex prediction given in Table 4.[42].

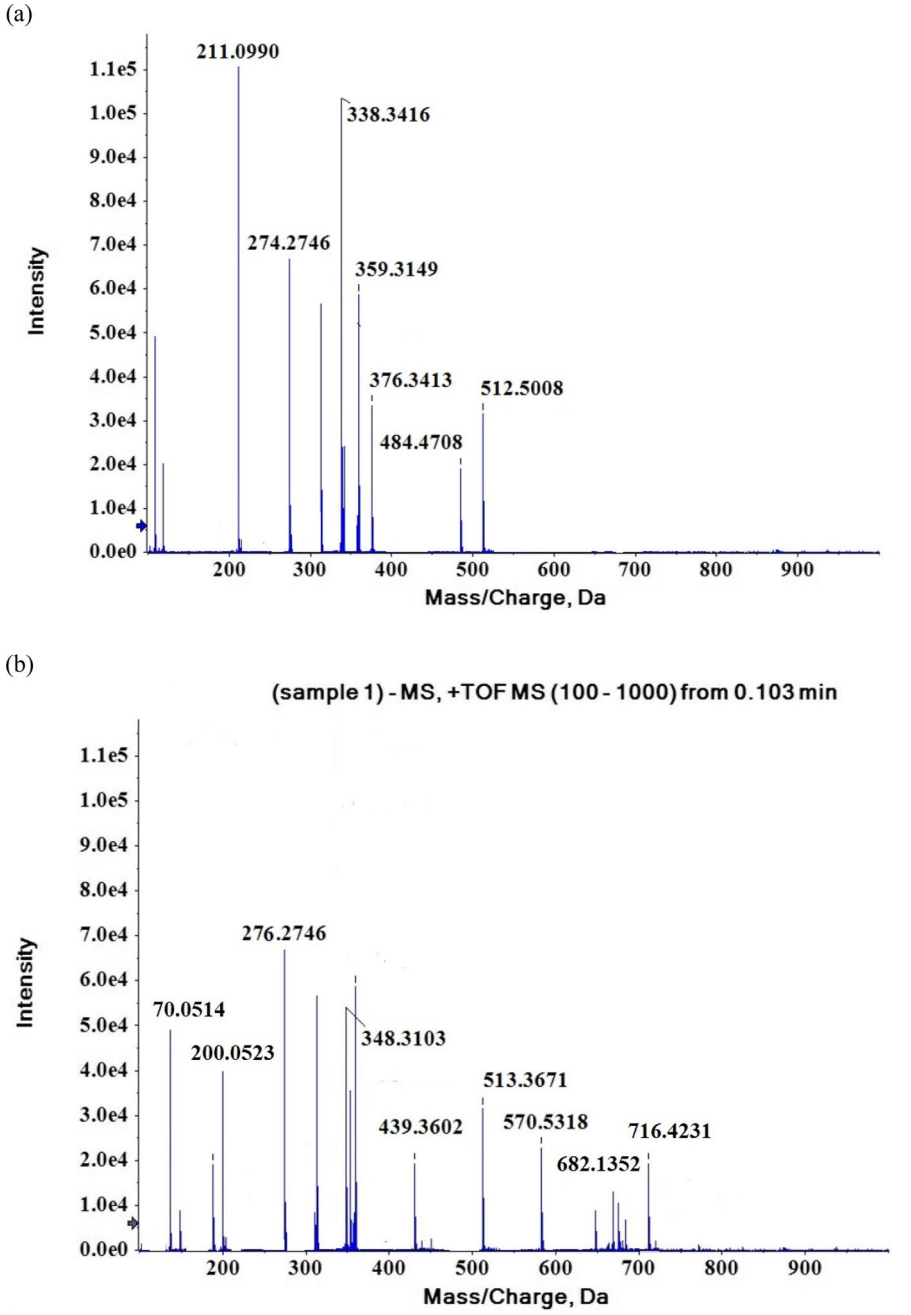

Fig. 4 **a** EI-MS spectra of ligand ($TAMacL_1$), **b** complex $[Ru(TAMacL_1)Cl_2]Cl$

Table 4 UV–Vis data ligands and Ru(III) complexes

Compound	$\mu_{eff.}$ (BM)	λ_{max} (cm^{-1})
$TAMacL_1$	–	272,379
$TAMacL_2$	–	284,395
$TAMacL_3$	–	276,388
$[Ru(TAMacL_1)Cl_2]Cl$	1.73	449,539
$[Ru(TAMacL_2)Cl_2]Cl$	1.85	451,542
$[Ru(TAMacL_3)Cl_2]Cl$	1.88	432,531

EPR spectra of Ru(III) complexes

The low spin t_{2g}^5 configuration for the Ru(III) complexes was suggested by magnetic moment values for complexes. The magnetic moment values for the complexes $[Ru(TAMacL_1)Cl_2]Cl$, $[Ru(TAMacL_2)Cl_2]Cl$, and $[Ru(TAMacL_3)Cl_2]Cl$ at (RT) room temp. have been measured, and the values obtained were 1.83 B.M., 1.85 B.M., and 1.88 B.M., respectively. These values correspond to one unpaired electron. At room temperature, the EPR spectra of Ru(III) macrocyclic complexes were obtained in the X-band. Because the measured 'g' values are particularly sensitive to tiny changes in structure and metal–ligand covalency, the low spin d^5 configuration is a great way to study molecule structure and bonding. The complexes' EPR spectra show the characteristics of distorted geometry with $g_\perp$ about 2.12–2.26 and $g\|$ around 1.81–1.96. These data show tetragonal distortion in the complexes for an octahedral field with tetragonal distortion $g_x = g_y \neq g_z$ given in Table 5. The position of lines and the type of macrocyclic ruthenium complexes' EPR spectra explained the distorted octahedral geometry of low spin ruthenium(III) complexes [43].

TGA

The thermogram curves of macrocyclic ligands ($TAMacL_1$–$TAMacL_3$) and Ru(III) complexes were carried out in the temperature range 40–800 °C under N_2 gas flow at 10 °C/min. In the temperature range of 90 to 200 °C, there is no weight loss, which excludes the presence of coordinated or uncoordinated water molecules. Due to the elimination of chloride anions, all of the complexes tested experience first step disintegration with weight losses of 10.12–19.35% (about 10.12–19.35%) at 230–250 °C. Due to the loss of the entire ligand, the complexes exhibit experimentally 56.23–64.86% (about 56.18–63.88%) second step breakdown in the

Table 5 EPR data for amide-based Ru(III) complexes

Complex	g_x	g_y	g_z	g^*
$[Ru(TAMacL_1)Cl_2]Cl$	2.23	2.23	1.96	2.14
$[Ru(TAMacL_2)Cl_2]Cl$	2.26	2.26	1.93	2.15
$[Ru(TAMacL_3)Cl_2]Cl$	2.12	2.12	1.81	2.02

$g^* = [1/3(g_x)^2 + 1/3(g_y)^2 + 1/3(g_z)^2]^{1/2}$

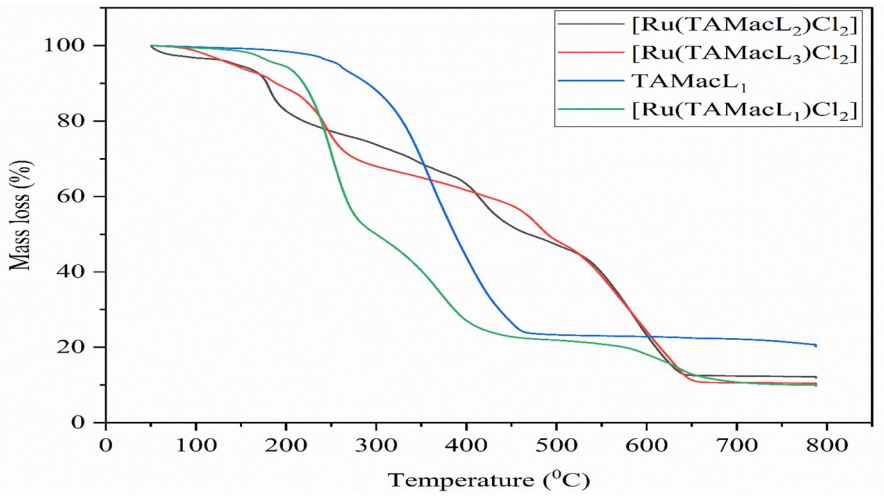

Fig. 5 Thermo-gravimetric analysis of macrocyclic ligands and Ru(III) complexes

temperature range 280–560 °C shown in Fig. 5. The final residue's metal oxide content was determined by IR spectra and matches the calculated amount.

Using Coats-Redfern and FWO (Figures S12–S17), the heat of activation (E_a) was computed for the number of breakdown stages from the TG and DTG in order to analyse the nature of metal ions on thermal conduct and the influence of the structural properties of the chelating agents. The composition approach was considered as a first-order reaction, and the activation order parameters were calculated using the Eyring equation. Tables S2 and S3 illustrate the results. [44]

Kinetic parameters

The activation energy obtained by the Kissinger methodology is equivalent to the activation energy discovered by the (O.F.W. method and C. R integral method. The equation was used to determine the thermodynamic parameters, including the Arrhenius factors (ΔH), (A), (ΔS) and (ΔG), after the kinetic study.

$$A = \frac{\beta \times E_a \times e^{\left(\frac{E_a}{RT_{max}}\right)}}{RT_{max}^2} \tag{1}$$

$$\Delta G = E_a + R \times T_{max} \ln\left(\frac{K_B T_{max}}{hA}\right) \tag{2}$$

$$\Delta H = E_a + RT_{max} \tag{3}$$

$$\Delta S = \frac{\Delta G - \Delta H}{T_{\max}} \tag{4}$$

where h represents the Planck constant (6.626×10^{-34} Js^{-1}) and kB represents the Boltzmann factor (1.38 10^{-23} Js^{-1}). At various heating rates, the Arrhenius factor was calculated using a variety of kinetic approaches. The results of (ΔS), (ΔH) and (ΔG) were furthered using a heating rate of 10 °C/min using a novel kinetic technique. The positive values of (ΔH) and (ΔG) show that the thermal breakdown of ligands ($TAMacL_1$–$TAMacL_3$) and related Ru (III) macrocyclic complexes is endergonic, unfavourable, and non-spontaneous [45].

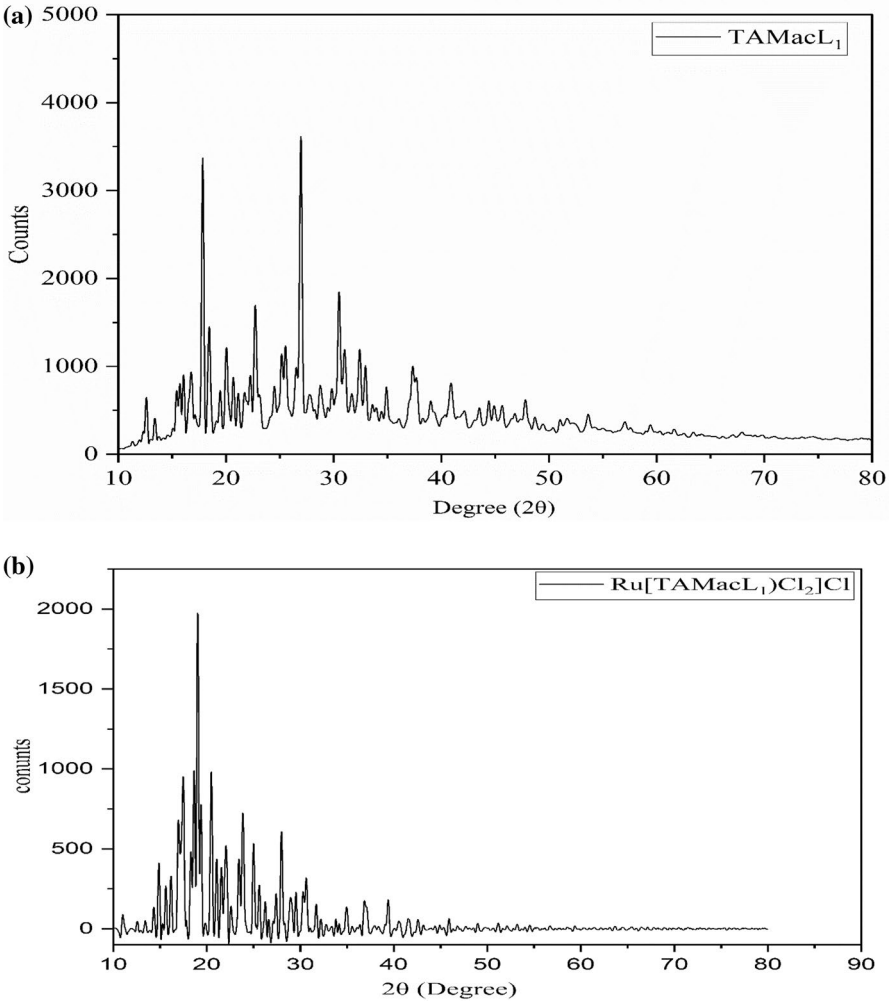

Fig. 6 **a** PXRD data of $TAMacL_1$, **b** PXRD data of $[Ru(TAMacL_1)Cl_2]Cl$

Table 6 Particular DFT bond lengths (Å) of macrocyclic ligands ($TAMacL_1$–$TAMacL_3$) and complexes [$Ru(TAMacL_1)Cl_2$–$Ru(TAMacL_3)Cl_2$]

Compound	(C=O)	(C–N)	(N–H)	(Ru–N)	(Ru–Cl)
$TAMacL_1$	1.22247	1.36596	1.01933	–	–
$TAMacL_2$	1.22194	1.36944	1.02737	–	–
$TAMacL_3$	1.21916	1.37549	1.01694	–	–
[$Ru(TAMacL_1)Cl_2$]	1.24824	1.60058	1.04697	2.88311	2.24222
[$Ru(TAMacL_2)Cl_2$]	1.22229	1.42752	1.02754	2.13128	2.42616
[$Ru(TAMacL_3)Cl_2$]	1.22446	1.43013	1.0303	2.21431	2.41806

Table 7 Particular DFT bond angles (°) of macrocyclic ligands ($TAMacL_1$–$TAMacL_3$) and complexes [$Ru(TAMacL_1)Cl_2$–$Ru(TAMacL_3)Cl_2$]

Atoms connectivity	Bond angle (°)	Atoms connectivity	Bond angle (°)
N–Ru–Cl	90.3080	N–Ru–Cl	90.3074
N–Ru–N	81.8330	N–Ru–Cl	90.8356
N–Ru–Cl	88.7333	N–Ru–Cl	90.1056
N–Ru–N	96.9572	N–Ru–Cl	90.1052
N–Ru–Cl	88.7308	Cl–Ru–Cl	178.7294
N–Ru–Cl	96.9565		
N–Ru–N	178.7124		
N–Ru–N	84.2567		
N–Ru–N	90.8383		

PXRD analysis

The structural characterisation and lattice size determination were done using the powder X-ray diffractogram of the ligands ($TAMacL_1$–$TAMacL_3$) and Ru(III) complexes (Fig. 6). The observed data for the complexes under research were compared to other data from the literature that had comparable cells, and then, they were indexed to the same geometry. Macrocyclic ligands ($TAMacL_1$–$TAMacL_3$) and Ru(III) complexes X-ray diffractograms were scanned in the $2\theta = 10°$–$90°$ range at 1.540A wavelength. The diffractogram and related data show the interplanar spacing (*d*-values), relative intensity, and 2 values for each peak. A computer programme has been used to index the X-ray diffraction pattern of these compounds in relation to significant peaks with relative intensities larger than 10% [45]. The parameters of unit cell of the complex [$Ru(TAMacL_1)Cl_2$]Cl were $a = 14.6495$, $b = 17.7782$, $c = 8.5463$ with $\alpha = \beta = \gamma = 90°$. The condition $a \neq b \neq c$ and $\alpha = \beta = \gamma = 90°$ of macrocyclic complex was in well accordance with orthorhombic crystal systems and octahedral geometry were confirmed. According to the PXRD results, the ligands, behave as tetradentate chelating agents. Furthermore, as the Cl^- anions are coordinated to the ruthenium atom, a hexacoordinated environment for ruthenium has been postulated.

Molecular modelling

The bond lengths in ligand $TAMacL_1C{=}O$ and C–N (1.24842 and 1.60058 Å) become longer in Ru(III) complex (1.24842 and 1.60058 Å); this confirms that ruthenium atom coordinates to (C–N–H) group of the ligand. These values of bond lengths of ligands ($TAMacL_1$–$TAMacL_3$) and their complexes [$Ru(TAMacL_1)Cl_2$–$Ru(TAMacL_3)Cl_2$]Cl calculated using density functional theory (DFT) given in Table 6. The bond angle (º) readings for the examined complexes [$Ru(TAMacL_1)Cl_2$–$Ru(TAMacL_3)Cl_2$] given in Table 7 have confirmed the hexacoordinated environment around the central meatal atom, *i.e*. octahedral geometry of the complexes and the results were also supported the postulated structure (Fig. 7)[46].

Quantum chemical calculations

Numerous quantum chemical reactivity descriptors that are used to assess chemical reactivity in addition to the uniqueness of the reactive site in chemical systems are effectively quantified using the density functional theory (DFT). The optical characteristics, stability, chemical reactivity, and electrical properties are investigated and described using frontier molecular orbitals. Electron excitation moves from HOMO to LUMO with the help of the roles of donor and acceptor, HOMO and LUMO. In this work, B3LYP/def2svp was used to quantify the FMOs energies, i.e. E_{HOMO}, E_{LUMO}, and their energy gaps (Figs. 8 and 9) E_{HOMO}–E_{LUMO} of the macrocyclic ligands ($TAMacL_1$–$TAMacL_3$) and their Ru(III) complexes [$Ru(TAMacL_1)Cl_2$–$Ru(TAMacL_3)Cl_2$], represented in Fig. 10 [47, 48].

A reactive, soft, and unstable chemical system was one with a low ΔE (The HOMO–LUMO energy gap) value. Because the computed global softness (S) values for the examined compounds were lower than the calculated global hardness (η), the synthesised amide macrocyclic ligands ($TAMacL_1$–$TAMacL_3$) were comparatively

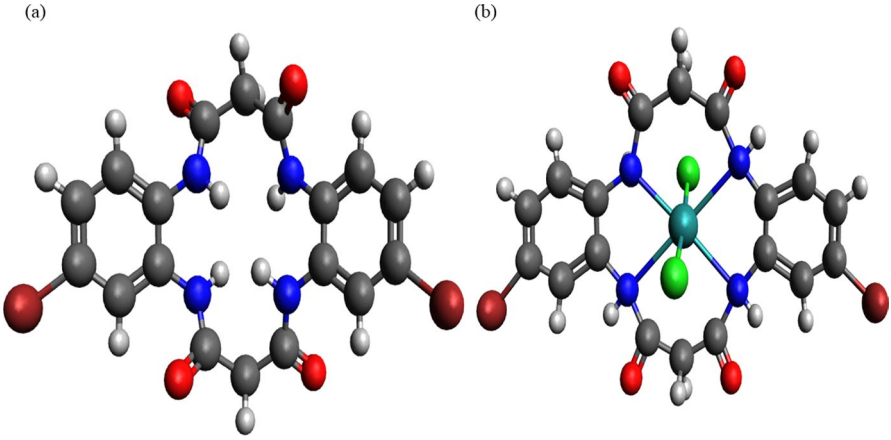

Fig. 7 Optimised structure of macrocyclic ligand $TAMacL_1$ and complex [$Ru(TAMacL_1)Cl_2$]Cl

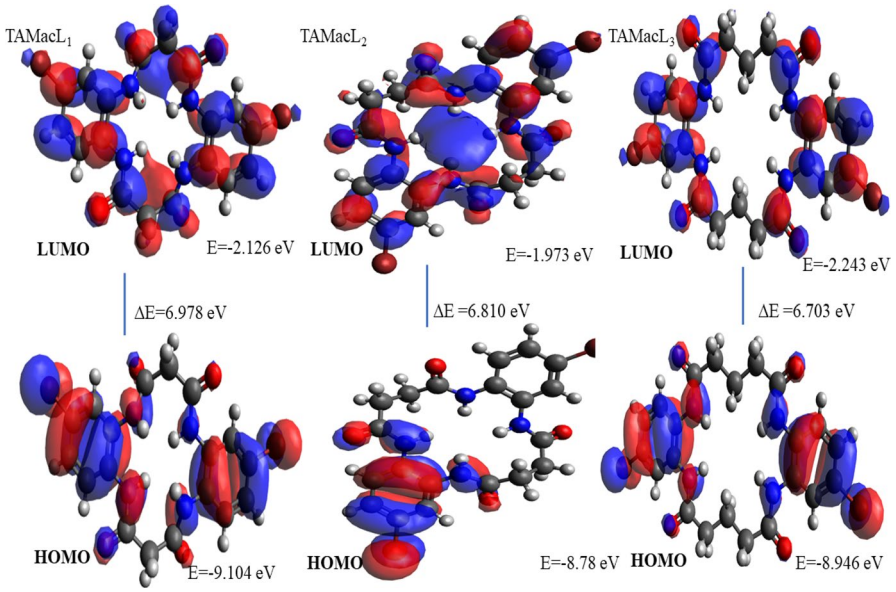

Fig. 8 E_{HOMO}–E_{LUMO} energy gap of the ligands ($TAMacL_1$–$TAMacL_3$)

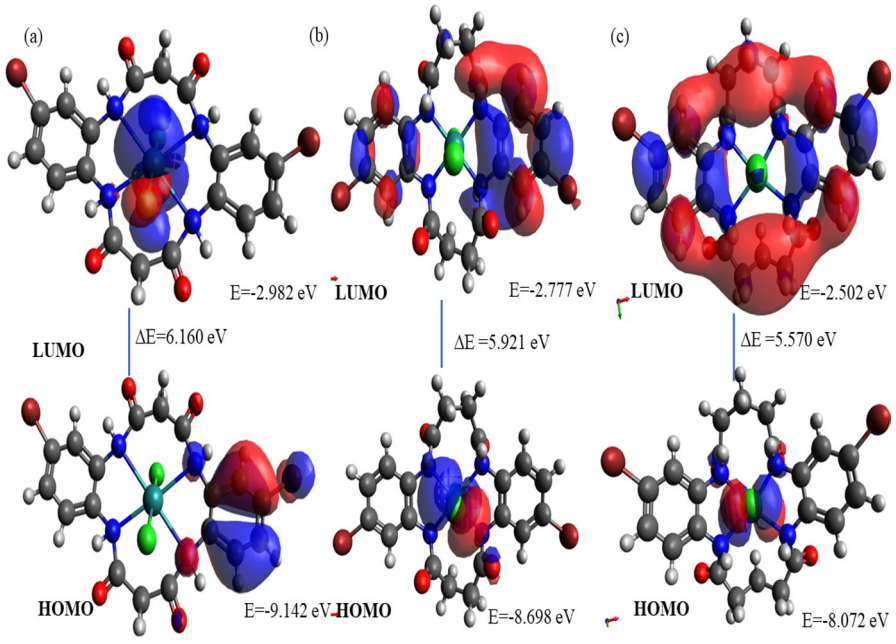

Fig. 9 E_{HOMO}–E_{LUMO} energy gap of Ru(III) complexes

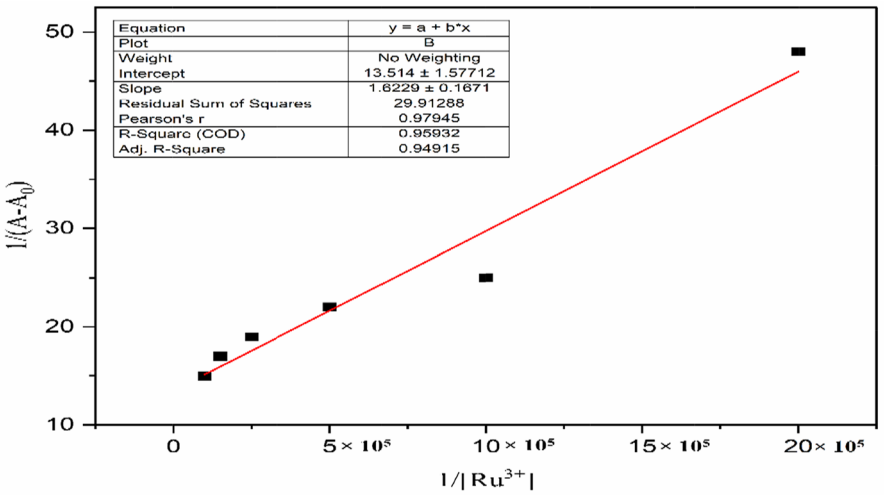

Fig. 10 Benesi–Hildebrand plots for determination of binding constant (10 µM) with Ru^{3+} concentration

Table 8 Theoretically premeditated global parameters of the compounds

Parameters	($TAMacL_1$)	($TAMacL_2$)	($TAMacL_3$)	6(a)	6(b)	6(c)
E_{HOMO} (eV)	−9.104	−8.783	−8.946	−9.142	−8.698	−8.072
E_{LUMO} (eV)	−2.126	−1.973	−2.243	−2.982	−2.777	−2.502
ΔE (eV)	6.978	6.810	6.703	6.160	5.921	5.570
IE (eV)	9.104	8.783	8.946	9.142	8.698	8.072
χ (eV)	5.615	5.378	5.5945	6.062	5.7375	5.287
η (eV)	3.489	3.405	3.3515	3.08	2.9605	2.785
S $(eV)^{-1}$	0.1433	0.1468	0.1491	0.1623	0.1688	0.1795
ω (eV)	4.518	4.2471	4.518	5.9655	5.5596	5.0183
Pi	−5.615	−5.378	−5.5945	−6.062	−5.7375	−5.287

stable and unreactive [49]. The examined metal complexes [Ru($TAMacL_1$)Cl_2–Ru($TAMacL_3$)Cl_2]Cl, may have better electron-donating capability than ligands and certain conventional compounds, as evidenced by the lower electron-contributing ability of the compounds with the lowest values of E_{HOMO}. The macrocyclic complex [Ru($TAMacL_3$)Cl_2]Cl is highly reactive as compare to other macrocyclic compounds with $\Delta E = 5.570$ given in Table 8 [50]. These findings led to the conclusion that metal complexes would be superior candidates for biological activity and antioxidants.

Determination of binding constant by Benesi–Hildebrand method

The Benesi–Hildebrand equation [51] was used to get the binding constant, and the equation below was used to calculate K_α.

$$1/(A - A_o) = 1/\{K(A_{max} - A_o)\,[M^{x+}]^n\} + 1/[A_{max} - A_o]$$

Here, K_α represents the binding constant, A represents the absorbance when the added guest is presented, A_o represents the absorbance when the added guest is absent, and A_{max} represents the absorbance when the added $[M^{x+}]$max present, where $[M^{X+}]$ is $[Ru^{3+}]$. The slope of the straight line plotting $1/(A-A_o)$ versus $1/[Ru^{3+}]$ might be used to calculate the binding constant (K_α) and is found to be 5.86×10^5 M^{-1}. The higher value of binding constant 5.86×10^5 M^{-1} indicates the strong interaction with Ru^{3+} ion (Fig. 10).

Biological activities

Antimicrobial activity

The antimicrobial efficacy of all the novel series of macrocyclic ligands ($TAMacL_1$–$TAMacL_3$) and their Ru(III) complexes [$Ru(TAMacL_1)Cl_2$–$Ru(TAMacL_3)Cl_2$] metal chelates was assessed in contrast to Gram+ve bacteria (*Streptococcus mutans* and *Staphylococcus aureus*), Gram−ve bacteria (*Klebsiella pneumoniae* and *Escherichia coli*) and fungal strains (*Fusarium oxysporum* and *Candida albicans*) for their in vitro antimicrobial potential, while Gentamicin, Ampicillin, and Nystatin were used as standard drugs for bacterial and fungal strain, respectively. The outcomes (Table 9) and some of the tested plates are displayed. seen in Figure S25., At 15 mg/ml (Fig. 11a, b), preliminary screening was conducted. It was discovered that macrocyclic complex $[Ru(TAMacL_3)Cl_2]Cl$ showed higher antibacterial activity with the zones of inhibition of 25.8 mm against *S. mutans*, 21.5 mm against *S. aureus* and complex $[Ru(TAMacL_2)Cl_2]Cl$ showed higher activity with zone of inhibition of 23.8 mm against *E. coli* and 22.4 mm against *K. pneumonia*. The impermeability of the microbes' cells or variations in

Table 9 Antimicrobial agar diffusion assay of macrocyclic ligands and their Ru(III) complexes: diameters (mm) of inhibition zones (% of standard)

	Gram−ve bacteria		Gram+ve bacteria		Fungi	
Compounds	*E. coli*	*K. pneumonia*	*S. aureus*	*S. mutans*	*C. albicans*	*F. oxysporum*
$TAMacL_1$	15.7	16.5	14.3	15.6	14.4	15.3
$TAMacL_2$	16.2	16.8	15.4	16.7	16.7	15.7
$TAMacL_3$	16.4	16.4	15.5	15.4	15.4	16.5
$[Ru(TAMacL_1)Cl_2]$	23.7	21.6	20.1	23.7	23.7	22.9
$[Ru(TAMacL_2)Cl_2]$	23.8	22.4	20.4	23.9	23.9	23.1
$[Ru(TAMacL_3)Cl_2]$	23.6	22.3	21.5	25.8	25.8	23.5
Gentamicin	27	25	–	–	–	–
Ampicillin	–	–	22	30	–	–
Nystatin	–	–	–	–	21	26

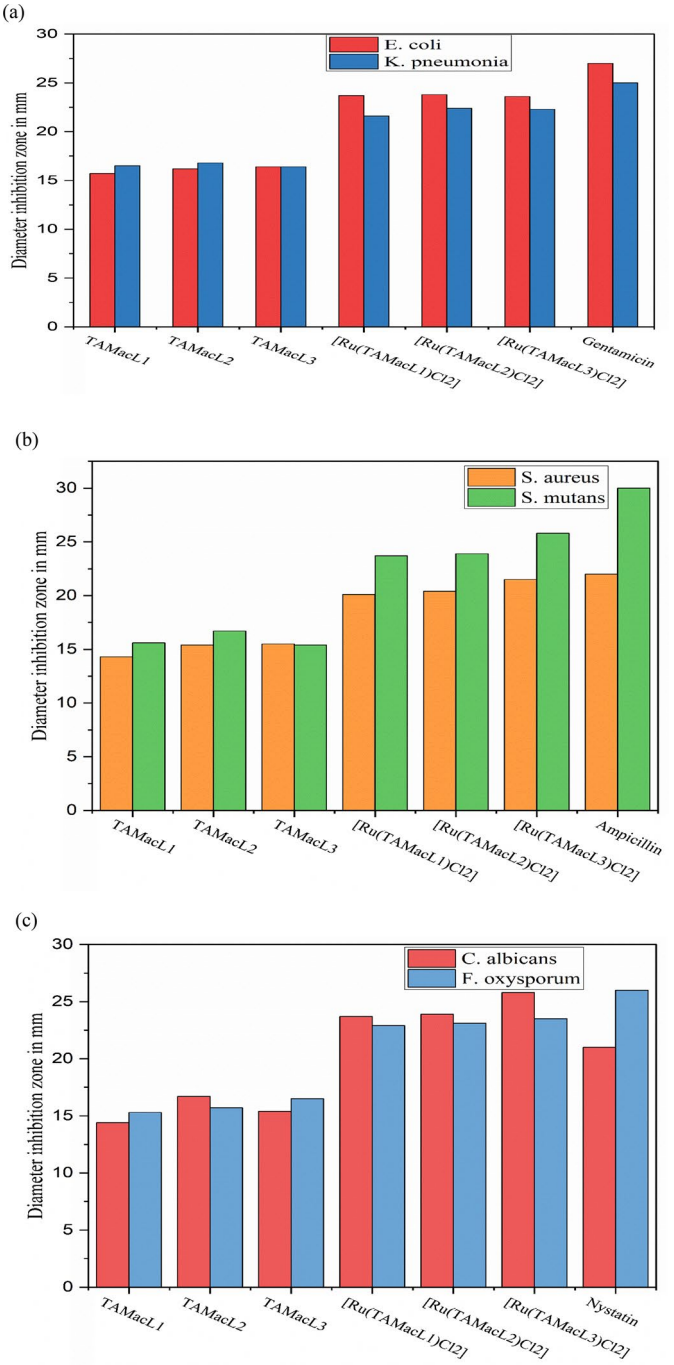

Fig. 11 Antibacterial (**a**, **b**) and antifungal (**c**) activity of the ligands and their Ru(III) complexes [diameter of inhibition zone in mm]

the ribosome of microbial cells cause the variance in $[Ru(TAMacL_2)Cl_2]Cl$ antibacterial efficacy against the two pathogens. The size of the inhibitory zone in the complexes under study showed that the kind of divalent cation has an impact on the antibacterial activity of $[Ru(TAMacL_2)Cl_2]Cl$. Similarly, the macrocyclic complex $[Ru(TAMacL_3)Cl_2]Cl$ showed higher antifungal activity with 25.8 mm inhibition of zone against *C. albicans* and 23.5 mm against *F. oxysporum* at 15 mg/ml. (Fig. 11c). In contrast to the non-electrolytic behaviour of ligands, it is important to confirm that the maximum activity of $[Ru(TAMacL_{1\text{-}3})Cl_2]Cl$ complexes [52] may be linked to its ionic character. A survey of the macrocyclic compounds reported so far by earlier investigators indicates that the macrocyclic ligands and their transition metal complexes possesses potent antimicrobial property. The antimicrobial action of the complexes of Zn(II), Ni(II), and Co(II) had the highest average activity than their respective ligands reported by Sumrra et al. [52, 53] The findings of the current study showed superiority over the reported compounds.

Metal chelates often exhibit such antibacterial action because the metal ions they contain are lipophilic [53]. Additionally, the chelates may prevent microbial cells from respirating. As a result, the microbial cells will not be able to make the proteins necessary to stop the organism from growing further. This subsequently supported the idea that chelation improves antibacterial action. On the other hand, ground-state features can be related to the biological activity of the produced complexes. Table 6 shows that the largest value of dipole moment is found in Ru (III) complexes. This discovery could be a contributing factor to the strong action of Ru (III) complexes [54]. The presence of a greater number of chloride ions in Ru(III) complexes, where Ru(III) includes $3Cl^-$, may also play a significant role in their increased activity [55]. This chloride ion may facilitate the synthesis of hypochlorous acid, which then breaks down into HCl and O_2. The oxygen destroys the microorganisms by oxidising the biological components. Additionally, the interaction of the chloride ion with membrane proteins and enzymes may help to explain why there is a greater activity when Cl^- is present.

Table 10 Antioxidant activity of ligand and its metal complexes along with standard BHA, TBHQ

Compounds	Conc. (ppm)			IC_{50}
	100	200	300	
$TAMacL_1$	26.21	34.56	38.35	0.414
$TAMacL_2$	27.36	35.62	39.54	0.402
$TAMacL_3$	27.50	35.80	39.95	0.398
$[Ru(TAMacL_1)Cl_2]$	40.23	52.63	65.32	0.211
$[Ru(TAMacL_2)Cl_2]$	41.72	53.45	66.42	0.205
$[Ru(TAMacL_3)Cl_2]$	42.12	53.65	66.86	0.208
BHA, 200 ppm	–	89.80	–	–
TBHQ, 200 ppm	–	92.87	–	–

Antioxidant activity

The capacity of the synthesised macrocyclic ligands ($TAMacL_1$–$TAMacL_3$) and their Ru(III) complexes to scavenge the stable DPPH (2,2-diphenyl-1-picryl hydrazyl) radical is used to assess their antioxidant activity. Spectrophotometric analysis was used to measure the DPPH scavenging capability. Free radicals are often created by a variety of bio-redox pathways and have been connected to the ageing process in various chronic, life-limiting disorders including cancer, myocardial infarction, cataracts, etc. As a result, efforts to lessen the harm these species do are being embraced as the basis for cutting-edge treatment approaches. Table 10 lists the ligand's and its metal complexes' % antioxidant activity. The ability of synthetic compounds to scavenge the stable radical DPPH or donate hydrogen was used to measure their antioxidant activity. The UV–Vis spectrophotometer can measure the DPPH's transformation from purple to yellow following reduction by measuring the decline in absorbance at 517 nm. The ability of the macrocyclic compounds to scavenge free radicals was compared to that of the well-known natural antioxidant ascorbic acid shown in Fig. 12. In comparison with macrocyclic ligands ($TAMacL_1$–$TAMacL_3$), the macrocyclic Ru(III) complexes [$Ru(TAMacL_1)Cl_2$–$Ru(TAMacL_3)Cl_2$] showed superior antioxidant activity due to the coordination of ligand with metal ion [56]. The antioxidant potency (IC_{50}) follows the order ascorbic acid > [$Ru(TAMacL_3)Cl_2$] > [$Ru(TAMacL_2)Cl_2$] > [$Ru(TAMacL_3)Cl_1$] > $TAMacL_3$ > $TAMacL_2$ > $TAMacL_3$.

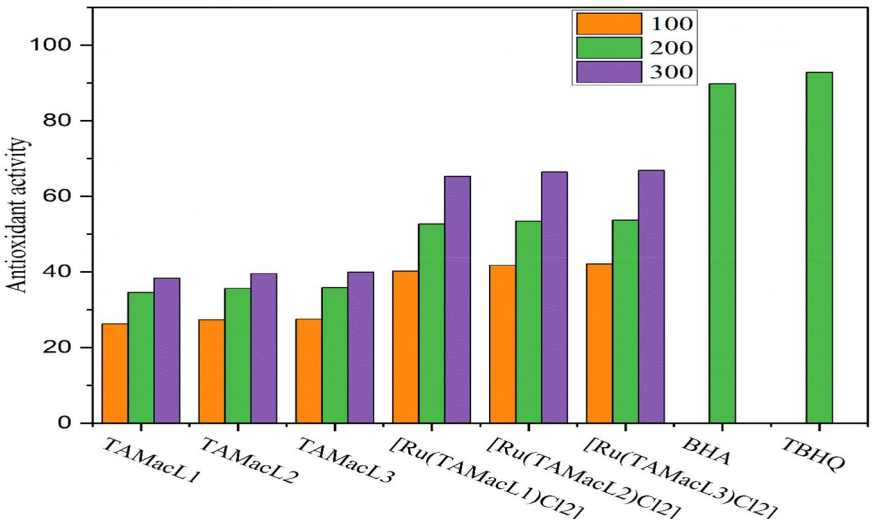

Fig. 12 The scavenging activity at various concentrations of the tetraamide macrocyclic ligands and Ru(III) Complexes with DPPH radical

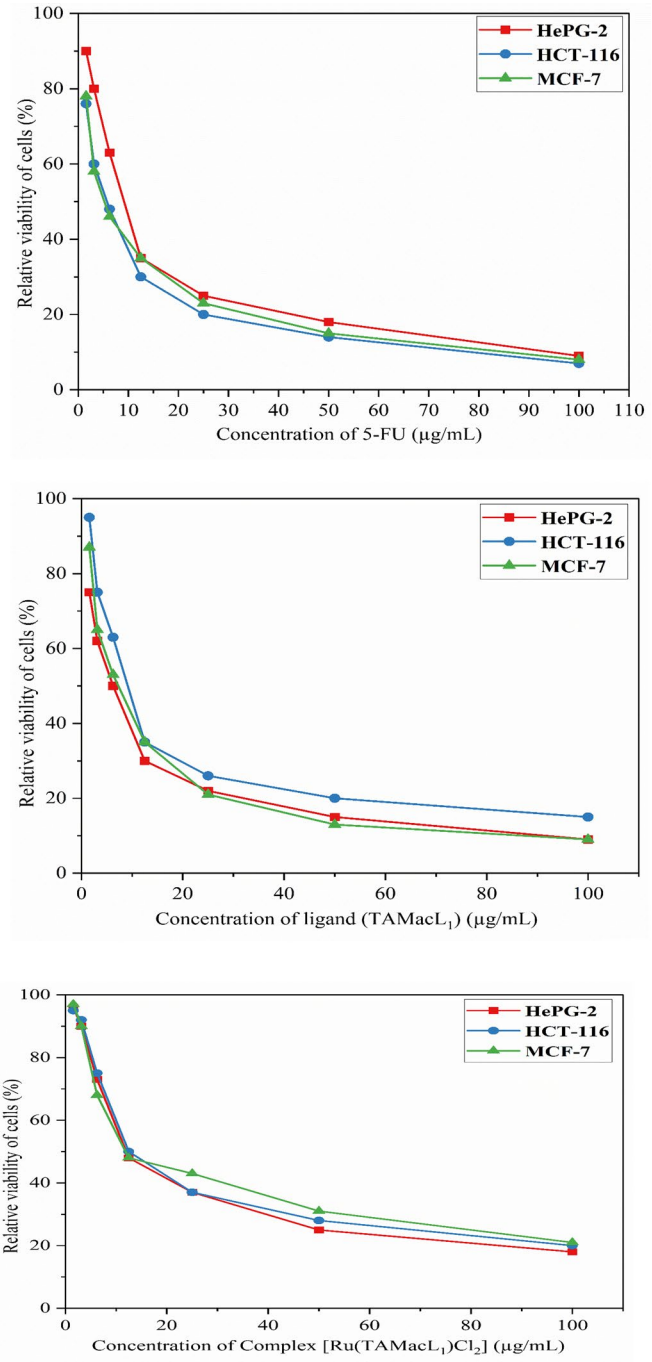

Fig. 13 Survival curve of the tumour call line for 5-fluorouracil, ($TAMacL_1$) and Ru(III) complex [$Ru(TAMacL_1)Cl_2$]

Table 11 IC_{50} (uM) value of cytotoxic efficacy of macrocyclic ligands and Ru(III) complexes

Compound	HePG-2	HCT-116	MCF-7
$TAMacL_1$	29.69 ± 0.23	19.13 ± 0.24	20.16 ± 0.31
$TAMacL_2$	27.43 ± 0.36	18.68 ± 0.32	19.56 ± 0.40
$TAMacL_3$	27.13 ± 0.26	18.59 ± 0.24	19.05 ± 0.35
$[Ru(TAMacL_1)Cl_2]$	9.21 ± 0.18	8.36 ± 0.19	7.54 ± 0.21
$[Ru(TAMacL_2)Cl_2]$	9.06 ± 0.34	8.12 ± 0.18	8.02 ± 0.32
$[Ru(TAMacL_3)Cl_2]$	9.13 ± 0.12	7.42 ± 0.24	7.12 ± 0.18
5-Fu	7.9 ± 0.28	5.2 ± 0.14	5.5 ± 0.21

Cytotoxicity

Employing a colorimetric MTT assay, cytotoxic activity was accessed for macrocyclic ligands ($TAMacL_1$–$TAMacL_3$) and their Ru(III) complexes against three distinct human cancer cell lines, HePG2, HCT116, and MCF7. The mitochondrial dehydrogenase activity is measured using this technique to assess the viability of cells. The growth inhibitory concentration value (IC_{50}) was used to explain the cytotoxicity results. This shows the amount of the chemicals needed to result in a 50% reduction in cell growth compared to untreated controls after 72 h of incubation. IC_{50} values have been calculated using the cancer cell line's survival curve. For each test compound, concentrations of 1.56, 3.125, 6.25, 12.5, 25, 50, and 100 g/ml were recognised shown in Fig. 13. 5-fluorouracil is used as reference, and the findings of IC_{50} conc. of ligands ($TAMacL_1$–$TAMacL_3$) and their Ru(III) complexes were compared with this, shown in Table 11. The values ± SD were given by calculating the average of three separate experiments. According to the findings, ruthenium-based macrocyclic complexes are more effective against the cancer cell lines as compared to the ligands. The metal complexes Ru(III) showed potential cytotoxic activity greater than the ligands $TAMacL_3$. In comparison with the ligands $TAMacL_1$–$TAMacL_3$, the Ru(III) complexes demonstrated superior cytotoxic action against the HePG2 and HCF-7 cell lines (IC_{50} values of 9.06 and 7.42 g/ml, respectively) given in Table 11. Therefore, it may be inferred that this molecule might be employed in the development of novel anticancer medications. This outcome is consistent with Wang et al.'s study [57], in which they assessed the cytotoxicity of pyrazolone-based compounds against four cancer cell lines. The IC_{50} of the macrocyclic ligands and their Ru(III) complexes ranged from 9.06 to 29.69 g/ml, covering a wide range of cytotoxicity against the various cancer cell lines. This behaviour suggests that all complexes showed high to moderate anticancer activity against the cell lines.

In silico molecular docking study

When utilising the AutoDock Vina programme, docking experiments are used to determine the biocidal implication of the synthesised ligands [58]. The recovered PDB file (3T88, 6WII, 3TY7, 3L8R, 3DRA, and 8EBB) *E. coli* (3T88), *K. pneumonia* (6WII), *S. aureus* (3T47), and *S. mutans* (3L8R) were specified as antibacterial

Table 12 The binding affinity, binding mode and number of H-bonds of macrocyclic compounds

Compounds	Active protein (PDB ID)	Binding affinity (kcal/mol)	Number of H-bond	Binding mode
[$TAMacL_1$]	3T88	− 10.2	1	ASP'1598
	6WII	− 7.8	2	ARG'79, GLU'43
	3T47	− 10.5	2	LYS'403, GLY'405
	3L8R	− 7.7	1	THR'513
	3DRA	− 8.6	1	ILE'502
	8EBB	− 8.5	1	ASN'55
[$TAMacL_2$]	3T88	− 9.7	2	ASP'755, ASP'474
	6WII	− 7.9	1	ASP'48
	3T47	− 10.0	1	LYS'857
	3L8R	− 8.0	1	HIE'384
	3DRA	− 8.8	1	ASN'331
	8EBB	− 8.7	1	ASN'225
[$TAMacL_3$]	3T88	− 11.2	1	ASP'474
	6WII	− 8.0	2	ARG'86, GLN'85
	3T47	− 11.0	2	PHE'238, ASP'237
	3L8R	− 8.4	1	HIE'384
	3DRA	− 9.6	1	SER'128
	8EBB	− 10.0	2	ILE'128, ASN'225

target, *C. albicans* (3DRA) and *F. oxysporum* (8EBB) were specified as antifungal target was entered into Auto Dock Vina as an input and designated as a macromolecule that prepares the protein by adding charges and hydrogen bonds to the atoms. In the process of preparing the ligand, numerous tautomers were produced, bond ordering was assigned, ring conformations were created, and stereo chemistry of the ligand was carried out. All of the produced conformations were then employed for a docking investigation.

Selecting the active residues and the Run auto grid option created a receptor grid around the protein active region. Run Vina was used to do the docking calculations, and the result was utilised to find the optimal docked structure using the binding affinity. In kcal/mol, the anticipated binding affinity is shown. The binding score for the best docked complex, which indicates a good inhibition, is − 11.2 for the $TAMacL_3$ ligand against 3T88. For analysis, the one with the greatest binding affinity is taken into account. The binding affinities of various ligands with various receptors are displayed in Table 12 [59, 60].

The macrocyclic ligand $TAMacL_3$ showed upright interaction by the *Escherichia coli* protein.

Figure 14 depicts the analysis of protein–ligand interactions, including hydrogen bonding and hydrophobic interactions. The typical H-bonding interactions (green colour) are shown in residues with Asp755 residue within 3.03 Å and with Asp474 residue within 2.69 Å, respectively. Several nonpolar hydrophobic connections were exposed between the aromatic carbons of the ligand ($TAMacL_3$)

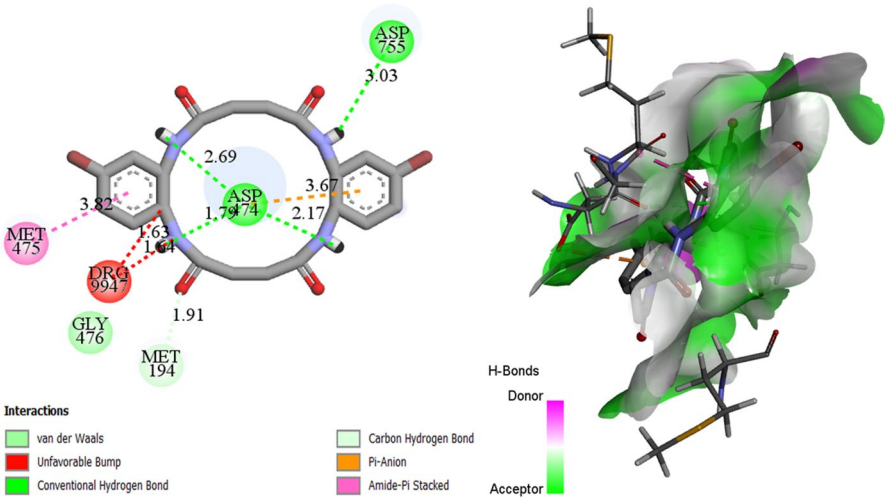

Fig. 14 **a** 2D plot of macrocyclic ligand $TAMacL_3$ with the protein receptor *E. Coli* (3T88), **b** 3D plot of ligand $TAMacL_3$

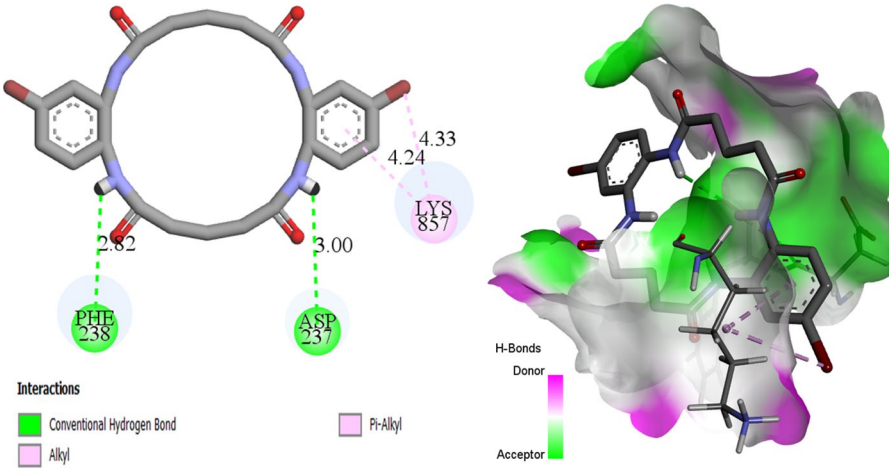

Fig. 15 **a** 2D plot of macrocyclic ligand $TAMacL_3$ with the protein receptor *S. aurous* (3TY7) and **b** 3D plot of ligand $TAMacL_3$

and Gly476, Met475, Met194 shown in Fig. 14. The best-docked ligand, $TAMacL_3$, has a binding energy of − 11.2 kcal mol^{-1} with the *E. coli* (3T88) protein binding site.

Similarly, the macrocyclic ligand $TAMacL_3$ showed good interactions with the *S. aurous* protein (3TY7). Typical H-bonding interactions (green colour) are shown in residues with Phe238 and Asp237 residue within 3.00 Å. Several non-polar hydrophobic interactions were discovered between the aromatic carbons

of the macrocyclic ligands and Lys857 shown in Fig. 15. The ligand, $TAMacL_3$ showed highest binding energy of − 11.00 kcal/mol with the *S. aurous* (3TY7) protein binding site.

Conclusion

In the present study, novel N4-tetraazamacrocyclic ligands ($TAMacL_1$–$TAMacL_3$) and their Ru(III) complexes [$Ru(TAMacL_1)Cl_2$–$Ru(TAMacL_3)Cl_2$] were synthesised. To characterise, several analytical and spectroscopic approaches were utilised and clarify the distorted octahedral geometry of the metal complexes. Also, DFT method was consistent with the experimental finding. The biological activity of the synthesised ligand and their complexes was studied against microbes for their in vitro antimicrobial potential. The results reviled that the macrocyclic complex [$Ru(TAMacL_3)Cl_2$]Cl showed higher antibacterial activity with the zones of inhibition of 25.8 mm against *S. mutans*, 21.5 mm against *S. aureus* and complex [$Ru(TAMacL_2)Cl_2$]Cl showed higher activity with 23.8 mm inhibition of zone against *E. coli* and 22.4 mm against *K. pneumonia* at 15 mg/ml. Similarly, Furthermore, the macrocyclic complex $Ru(TAMacL_3)Cl_2$] have higher ability to scavenge free DPPH radical. The antioxidant potency (IC_{50}) of the macrocyclic complex $Ru(TAMacL_3)Cl_2$] was 0.22 mg/mL, relative to ascorbic acid (IC_{50} = 0.12 mg/mL). By screening some of the compounds against three distinct human cancer cell lines, HePG2, HCT116, and MCF7, results showed that Ru(III) complexes demonstrated superior cytotoxic action against the HePG2 and HCF-7 cell lines (IC50 values of 9.06 and 7.42 g/ml, respectively). Molecular docking studies of the macrocyclic ligands and their Ru(III) complex with receptors of (PDB ID 3T88, 6WII, 3TY7, 3L8R, 3DRA, and 8EBB) detected that the ligand ($TAMacL_3$) showed lowest binding ability with binding energy of − 11.2 kcal mol^{-1} with the receptor of *E. coli* (PDB ID: 3T88). As a consequence, molecular docking investigations backed with the experimental findings of antimicrobial properties. As a result, they may be regarded as promising prospective medications for therapeutic intervention in a variety of disorders.

Supplementary Information The online version contains supplementary material available at https://doi.org/10.1007/s11164-023-05124-1.

Acknowledgements The author (Subhash) is highly thankful to the University Grants Commission, New Delhi, India, for financial assistance in the form of a Junior Research Fellowship (NTA Ref. No. 92, CSIR-UGC NET DECEMBER, 2018). The authors gratefully acknowledge DST-FIST programme 2017 (final proposal no. SR/FST/CS-I/2017/12(C) dated 10.5.2018, Department of Chemistry, Kurukshetra University, Kurukshetra) for providing financial support in form of NMR spectral studies. I am also thankful to Dr. Senthilkumar Muthaiah, NIT, Kurukshetra, for his goodwill and expert guidance.

Author contributions The idea was suggested by Subhash and Ashu Chaudhary. The experimental section was performed by Jyoti, Monika Gupta, and Anita Phor. Interpretation of data, preparing of the manuscript, and its editing were performed by Subhash. All authors reviewed the manuscript.

Funding The author (Subhash) is highly thankful to the University Grants Commission, New Delhi, India, for financial assistance in the form of a Junior Research Fellowship (NTA Ref. No. 92, CSIR-UGC NET DECEMBER, 2018).

Availability of data and materials All data are available in the article and its supplementary material.

Declarations

Conflict of interest The authors declare no conflict of interest.

Ethical approval Not applicable.

References

1. M. Dalal, A. Dubey, N. Antil et al., Res. Chem. Intermed. **49**, 2889–2917 (2023)
2. L. Ronconi, P.J. Sadler, Coord. Chem. Rev. **251**, 1633–1648 (2007)
3. S. Noreen, S.H. Sumrra, ACS Omega **6**(48), 33085–33099 (2021)
4. S.H. Sumrra, F. Mushtaq, F. Ahmad, R. Hussain, W. Zafar, M. Imran, M.N. Zafar, Chem. Pap. **76**(6), 3705–3727 (2022)
5. S. Khalid, S.H. Sumrra, Z.H. Chohan, JSM **49**, 1891 (2020)
6. S.H. Sumrra, M. Hanif, Z.H. Chohan, M.S. Akram, J. Akhtar, S.M. Al-Shehri, J. Enzyme Inhib. Med. Chem. **31**, 590 (2016)
7. S.H. Sumrra, M. Imran, M. Ibrahim, S. Ambreen, R. Mehmood, M.A. Assiri, A. Irfan, J. Chil. Chem. Soc **66**, 5057 (2021)
8. S.H. Sumrra, U. Habiba, W. Zafar, M. Imran, Z.H. Chohan, J Coord. Chem. **73**, 2838–2877 (2020)
9. M. Mitra, S.K. Seth, S.R. Choudhury, P. Manna, A. Das, M. Helliwell, A. Bauzá, A. Frontera, S. Mukhopadhyay, Eur. J. Inorg. Chem. **2013**, 4679–4685 (2013)
10. W. Zafar, S.H. Sumrra, Z.H. Chohan, Eur. J. Med. Chem. **222**, 113602 (2021)
11. N. Oliphant, R.J. Bartlett, J. Chem. Phys. **100**, 6550 (1994)
12. X.H. Wang, X. Kun Wang, Y.J. Liang, Z. Shi, J.Y. Zhang, L.M. Chen, L.W. Fu, Chin. J. Cancer. **29**, 980 (2010)
13. F.S. Al-Fartusie, S.N. Mohssan, Indian J. Adv. Chem. Sci. **5**, 127 (2017)
14. A. Krężel, W. Maret, Arch. Biochem. Biophys. **3**, 611 (2016)
15. M.S. Hossain, P.K. Roy, C.M. Zakaria, M. Kudrat-E-Zahan, Int. J. Chem. Stud. **6**, 19 (2018)
16. S. Naser, H. Samh, C. Mohamad, Damascus Univ. J. Basic Sci. **30**, 83 (2014)
17. P. Kamalakannan, D. Venkappaya, J. Inorg. Biochem. **90**, 22 (2009)
18. M.S. Islam, M.A. Farooque, M.A.K. Bodruddoza, M.A. Mosaddik, M.S. Alam, J. Biol. Sci. **2**, 797 (2002)
19. M. Selvaganapathy, N. Raman, J. Chem. Biol. Ther. **1**, 108 (2016)
20. L. Wang, C. Hu, L. Shao, Int. J. Nanomed. **12**, 1227 (2017)
21. E. Tfouni, F.G. Doro, A.J. Gomes, R.S. Silva, G. Metzker, P.G.Z. Benini, D.W. Franco, Coord. Chem. Rev. **254**, 355–371 (2010)
22. E. Tfouni, K.Q. Ferreira, F.G. Doro, R.S. da Silva, Z.N. da Rocha, Coord. Chem. Rev. **249**, 405–418 (2005)
23. Subhash, A. Chaudhary, Jyoti, M. Kumar, R. Solanki, J. Iran. Chem. Soc. **7**, 1–24 (2023)
24. A.I. Vogel, *A Text Book of Quantitative Inorganic Analysis*, 3rd edn. (Longmans, London, 1961), pp.433–441
25. D.P. Singh, V. Malik, R. Kumar, K. Kumar, J. Serb. Chem. Soc **75**(6), 763–772 (2010)
26. Subhash, X. Jyoti, Chaudhary, Res. Chem. Intermed. **49**(9), 1–30 (2023)
27. M. Ismael, A.-M. Abdel-Mawgoud, M.K. Rabia, A. Abdou, Inorg. Chim. Acta **505**, 119443 (2020)
28. M. Ismael, A.-M. Abdel-Mawgoud, M.K. Rabia, A. Abdou, J. Mol. Struct. **1227**, 129695 (2021)
29. J.J. Biemer, Ann. Clin. Lab. Sci. **3**(2), 135–140 (1973)
30. D.E. Hunt, H.J. Sandham, Appl. Microbiol. **17**(2), 329 (1969)
31. R.G. Mohamed, A.A. Makhlouf, S.A. Mosad, A.A. Abdel Aziz, S.M. El-Medani, R.M. Ramadan, J. Coord. Chem. **71**, 3665 (2018)
32. P. Skehan, R. Storeng, D. Scudiero, A. Monks, J. McMahon, D. Vistica, J.T. Warren, H. Bokesch, S. Kenney, M.R. Boyd, J. Natl. Cancer Inst. **82**, 1107 (1990)

33. H.J. Mauceri, N.N. Hanna, M.A. Beckett, D.H. Gorski, M.J. Staba, K.A. Stellato, K. Bigelow, R. Heimann, S. Gately, M. Dhanabal, G.A. Soff, V.P. Sukhatme, D.W. Kufe, R.R. Weichselbaum, Nature **394**, 287 (1998)
34. C.J. Dhanaraj, I.U. Hassan, J. Johnson, J. Joseph, R.S. Joseyphus, J. Photochem. Photobiol. B **162**, 115 (2016)
35. I. Ali, W.A. Wani, K. Saleem, Synth. React. Inorg. Met. Org. Chem. **43**, 1162–1170 (2013)
36. M.A. Ayoub, E.H. Abd-Elnasser, M.A. Ahmed, M.G. Rizk, J. Mol. Struct. **1163**, 379–387 (2018)
37. O.H. Shehab, A. Abdalhady, R.H. Al-Hiti, Am. Chem. Sci. J. **2**, 1–11 (2012)
38. P.M. Reddy, K. Shanker, R. Rohini, V. Ravinder, Int. J. ChemTech Res. **1**, 367–372 (2009)
39. Mamta, Subhash, Pinki, A. Chaudhary, J. Mol. Struct. **1275**, 134667 (2023)
40. M. Shakir, N. Bano, M.A. Rauf, M. Owais, J. Chem. Sci. **129**(12), 1905–1920 (2017)
41. W.C. Ellis, A.D. Ryabov, A. Fischer, J.A. Hayden, L.Q. Shen, E.L. Bominaar, T.J. Collins, J. Coord. Chem. **71**(11–13), 1822–1836 (2018)
42. S. Rani, S. Kumar, S. Chandra, Spectrochim. Acta Part A Mol. Biomol Spectrosc. **118**, 244–250 (2014)
43. R. Ramesh, N. Dharmaraj, R. Karvembu, K. Natarajan, Ind. J. Chem. **39A**, 1079 (2000)
44. O.A. El-Gammal, G.A. El-Reash, R.A. Bedier, Appl. Organomet. Chem. **33**(10), e5141 (2019)
45. V. Pushpanathan, S.S.J. Dhas, D.S. Kumar, Bull. Mater. Sci. **44**, 1–12 (2021)
46. M. Frezza, S. Hindo, D. Chen, A. Davenport, S. Schmitt, D. Tomco, Q.P. Dou, Curr. Pharm. Des. **16**, 1813 (2010)
47. Y.A. Alghuwainem, H.M.A. El-Lateef, M.M. Khalaf, A.A. Amer, A.A. Abdelhamid, A.A. Alzharani, A. Abdou, Int. J. Mol. Sci. **23**(24), 15614 (2022)
48. H. Hrichi, N.A. Elkanzi, A.M. Ali, A. Abdou, Res. Chem. Intermed. **49**(5), 2257–2276 (2023)
49. S. Shaaban, A. Abdou, A.G. Alhamzani, M.M. Abou-Krisha, M.A. Al-Qudah, M. Alaasar, T.A. Yousef, Life **13**(4), 912 (2023)
50. M.A. Arafath, F. Adam, M.B.A. Ahamed, M.R. Karim, M.N. Uddin, B.M. Yamin, A. Abdou, J. Mol. Struct. **1278**, 134887 (2023)
51. M. Dong, T.H. Ma, A.J. Zhang, Y.M. Dong, Y.W. Wang, Y. Peng, Dyes Pigm. **87**, 164–172 (2010)
52. S.H. Sumrra, W. Zafar, M. Imran, Z.H. Chohan, J. Coord. Chem. **75**(3–4), 293–334 (2022)
53. S. Noreen, S.H. Sumrra, Biometals **35**(3), 519–548 (2022)
54. M.A. I Al-Gaber, H.M. Abd El-Lateef, M.M. Khalaf, S. Shaaban, M. Shawky, G.G. Mohamed, A.M. Abu-Dief, Materials **16**(3), 897 (2023)
55. M.S. Hossain, K.A. Khushy, M.A. Latif, M.F. Hossen, M.A. Asraf, M. Kudrat-E-Zahan, A. Abdou, Russ. J. Gen. Chem. **92**(12), 2723–2733 (2022)
56. N.A. Elkanzi, H. Hrichi, H. Salah, M. Albqmi, A.M. Ali, A. Abdou, Polyhedron **230**, 116219 (2023)
57. W. Wang, Y.F. Li, X.W. Sun, Y. Chen, W. Li, D. Xu, Z. Zhou, Chin. J. Cancer **29**(11), 923–930 (2010)
58. O. Trott, A.J. Olson, J. Comput. Chem. **31**(2), 455–461 (2010)
59. N.A. Elkanzi, A.M. Ali, M. Albqmi, A. Abdou, Appl. Organomet. Chem. **36**(11), e6868 (2022)
60. A. Agrwal, R. Saini, S. Bhandri, S. Verma, P. Srivastava, O. Prakash, Mater. Today: Proc. **67**, 598–604 (2022)